Giant magnetoresistance dependence on the lateral correlation length of the interface roughness in magnetic superlattices

R. Schad*
Research Institute for Materials, KU Nijmegen, NL-6525 ED Nijmegen, The Netherlands

P. Beliën,† G. Verbanck, V. V. Moshchalkov, and Y. Bruynseraede
Laboratorium voor Vaste-Stoffysika en Magnetisme, KU Leuven, B-3001 Leuven, Belgium

H. E. Fischer
Institute Laue Langevin, 38042 Grenoble Cedex 9, France

S. Lefebvre and M. Bessiere
LURE, Université de Paris-Sud, 91405 Orsay Cedex, France
(Received 2 March 1998; revised manuscript received 6 August 1998)

The giant magnetoresistance (GMR) observed in magnetic multilayers, is due to spin-dependent electron transport. In order to study the influence of the interface roughness on the spin-dependent scattering we produced epitaxial Fe/Cr(001) superlattices with negligible bulk scattering. The interface roughness was varied by carefully annealing the samples. The vertical and lateral interface roughness components were quantitatively determined by specular and diffuse synchrotron x-ray diffraction using anomalous scattering. We find that the magnitude of the GMR effect increases with decreasing lateral correlation length ξ_x and increasing vertical roughness amplitude η. [S0163-1829(99)06001-4]

INTRODUCTION

The discovery of giant magnetoresistance (GMR) (Refs. 1–3) in Fe/Cr superlattices opened a new field of possible applications for artificially tailored materials. The effect is explained by spin-dependent electron transport[4–7] which results in different resistivities for the parallel and antiparallel configurations of the magnetization in adjacent magnetic layers. The antiparallel configuration is found in the absence of an applied magnetic field, provided that the Cr layer thickness is chosen to produce an antiferromagnetic (AF) exchange coupling. Application of an external field produces a ferromagnetic alignment leading to the resistance change. The dependence of the GMR amplitude on the structural properties of the superlattice is quite involved. Here several contributions have to be distinguished: (i) the magnetic structure, (ii) the spin-dependent electronic band structure, and (ii) spin-dependent electron scattering.

The magnetic structure is of importance because the full magnitude of the GMR effect is observed only when the magnetic configuration changes from fully antiparallel to parallel alignment. The latter will be easily achieved when the external magnetic field is strong enough to saturate the magnetization. The antiferromagnetic alignment at zero field, however, depends (in the case of an exchange coupled superlattice) on the nature of the exchange coupling and on superlattice imperfections in the form of pin holes. Instead of a simple antiferromagnetic alignment, the magnetization directions can form 90° angles between adjacent magnetic layers.[8] This will reduce the observed GMR by a factor of 2.[9] The strength of the 90° coupling is mediated by the interface roughness[10] or loose spins inside the spacer layers.[11] Thus, in both cases the magnitude of the GMR effect is linked to the interface quality via the exchange coupling. Magnetic pin holes (which are also a kind of structural defect) will cause ferromagnetic alignment of parts of the sample which consequently do not contribute to the GMR effect, thus diminishing its amplitude. Not only pin holes but also precursors of these in the form of larger spacer layer thickness fluctuations might lead to partially ferromagnetic alignment because of local changes of the exchange coupling. In spite of their structural origin these magnetic contributions are distinct from the pure electronic contributions and have to be separated experimentally by magnetization measurements. These give directly the fraction of the sample which is antiferromagnetically ordered (AFF) and does contribute to the GMR effect.

The other two contributions to the GMR effect, the spin-dependent electronic band structure and spin-dependent electron scattering, are the origin of the spin-dependent transport and form therefore the interesting part. They are, however, quite entangled. The electronic band structure on its own can generate a GMR effect without any spin-dependent scattering, for example in the limit of diluted scatterers[7] or in defect-free point contacts with ballistic transport.[12] This band structure contribution stems mostly from the asymmetry of the Fermi velocities for the two spin channels. Adding now spin-dependent scattering, the GMR effect can either be amplified or diminished depending on whether the scattering enhances or counteracts the band structure contribution. This spin asymmetry of the electron scattering is determined by, first, the density of states (DOS) available at the Fermi level and second, the spin asymmetry of the scattering potential. The DOS contribution, for instance, causes a spin asymmetry for any kind of electron scattering, even for phonon scattering.[13] In this way, the spin-dependent scattering also

includes band structure effects. For Cr impurities in Fe the scattering not only enhances but actually dominates the pure band structure contribution,[7] even in the dilute limit. In practice, due to the typically high defect densities in magnetic superlattices, the spin-dependent scattering contribution will likely dominate over the pure electronic band structure effects.

It is this spin-dependent scattering to which most publications, experimental and theoretical, are devoted. Here two contributions have to be considered separately, the spin-dependent scattering at impurities inside the magnetic layers (bulk scattering) and the scattering at the interfaces. Of course, both contributions can cause a GMR effect.[4-7] However, if both bulk and interface scattering are present at the same time, their spin asymmetry could be opposite. In that case the total spin asymmetry and hence the amplitude of the GMR effect would be reduced.[6] Polycrystalline samples naturally have a high degree of bulk defects with unknown spin asymmetry of the scattering potential. Since interface scattering is also important, this results in a rather involved system. Changing the structural quality of such samples will affect both bulk and interface properties causing unpredictable changes in the GMR. This effect may account for the contradictory experimental observations reported for polycrystalline samples.[14–19] In order to study the influence of the interface scattering alone on the GMR amplitude it is necessary to produce samples with negligible bulk scattering. This can be achieved by epitaxial growth of ultraclean materials on suitable substrates.[20,21] The interface quality can be altered by several methods of which annealing has certain advantages over others. For instance, ion bombardment necessarily introduces lots of bulk defects. Annealing experiments have been done before.[22–25] Usually it is observed that the GMR amplitude first slightly increases upon moderate annealing and then drops drastically towards zero. The decrease is caused by a loss of the AF order in the samples due to pin-hole formation which is easily understood yet not related to the spin-dependent transport. Thus far, the increase was only studied on samples with undefined bulk properties and therefore could not be related to changes of the interface structure. It is worth mentioning that a complete description of the interface structure must include both the vertical and lateral roughness components. Any structure analysis based on only one of these parameters is incomplete and cannot be expected to explain the behavior of the GMR effect.

In this paper we discuss the transport properties of epitaxial Fe/Cr(001) superlattices with exclusively interface electron scattering. Identical samples were prepared in a single deposition run to avoid any irreproducibility of the growth process. The interface quality was varied by annealing the samples at different (moderate) temperatures leading to an increase of the GMR amplitude. Quantitative analysis of the vertical and lateral interface structure is based on respectively specular and diffuse small angle (SA) x-ray diffraction (XRD) using a synchrotron source. The x-ray scattering contrast between Fe and Cr was enhanced through anomalous scattering, achieved by choosing the x-ray wavelength close to the absorption edge of Cr.

EXPERIMENTAL

The single-crystalline MgO(001) substrates[26] ($5\times15\ \mathrm{mm}^2$) showed micron-size flat terraces separated by atomic steps measured *ex situ* by atomic force microscopy (AFM). After rinsing in isopropyl alcohol and drying in a dry N_2 flow, the substrates were annealed at 600 °C in UHV for 15 min. The superlattices were prepared in a Riber MBE deposition system (2×10^{-11} mbar base pressure) equipped with electron beam evaporators, which were rate stabilized to within 1% by a home-made feedback control system[27] using Balzers quadrupole mass spectrometers (QMS). Additionally, integration of the QMS signal was used to control the shutters of the individual evaporation sources. Fe and Cr layers (starting material of 99.996% purity) were evaporated in a pressure of 4×10^{-10} mbar at a rate of 1 Å/sec on the MgO(001) substrates. The substrate temperature during the growth was 50 °C. The superlattices were deposited in a single deposition run on all substrates with the substrate holder rotated at 60 rpm. In this way, six identical samples were produced. Each superlattice consisted of 10 bilayers with 28 Å Fe and 11 Å Cr starting with a Fe layer. The whole stack was covered with an additional 20 Å Cr layer to protect the multilayer from oxidation.[28] All layers grew epitaxially with (001) orientation.[29] Afterwards the samples were annealed for 1 h in a vacuum of 10^{-8} mbar at various annealing temperatures (T_a) up to 460 °C: the temperature where pin-hole formation starts to destroy the AF coupling.

Structural information about the superlattices was obtained from SA XRD measurements performed at the LURE synchrotron light source (beamline D23) with wavelength 2.0753 Å (15 eV below the Cr absorption edge). The XRD spectra were measured in regular θ-2θ geometry and by ω rocks (rocking curves). Slight asymmetries in the ω rocks were removed by averaging left and right wing of the spectra. Quantitative values of the interfaces roughness were determined by simulating the spectra using the interface correlation function:[30–33]

$$C_{jk}(x)=\langle \delta z_j(x)\,\delta z_k(x)\rangle=\eta_j\,\eta_k e^{-(x/\xi_x)^{2h}} e^{-(\Delta z/\xi_z)^2}$$

with $\delta z_j(x)=z_j(x)-z_j$, the lateral and vertical correlation lengths ξ_x and ξ_z, and the average distance between the interfaces Δz. This function was successfully applied to experimental data before[34] and is closely related to models developed by other authors.[35–40] The vertical and lateral roughness parameters were obtained from, respectively, $\theta/2\theta$ scans and ω rocks. These include the roughness amplitude η, the lateral correlation length ξ_x (the characteristic lateral distance between ''bumps'' on a given interface), the vertical correlation length ξ_z (the distance between interfaces over which they lose their similarity), and the Hurst parameter h representing the jaggedness of the interface for a given ξ_x, as 3-h is the Hausdorf fractal dimension of the interface.

The electrical measurements were performed in an Oxford cryostat (1.5 up to 300 K) equipped with a 15 T magnet. Resistivities were determined using a standard four probe Van der Pauw method with the current and magnetic field in the plane of the film (CIP). The absolute and relative magnetoresistance are defined as $\Delta\rho=\rho_0-\rho_s$ and $\Delta\rho/\rho_s$, respectively, where ρ_0 is the resistivity in zero field and ρ_s the saturation resistivity. All quoted resistivity values were measured at 4.2 K.

Magnetization measurements were performed in a SQUID magnetometer at 4.2 K. The antiferromagnetic fraction

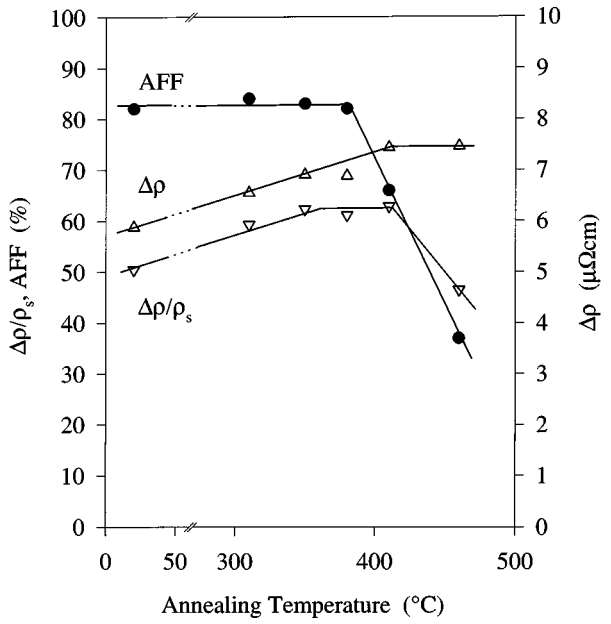

FIG. 1. Absolute and relative magnetoresistance ($\Delta\rho, \Delta\rho/\rho_s$) and the antiferromagnetic fraction (AFF) as a function of the annealing temperature. Note the break in the x axis. The lines are guides to the eye.

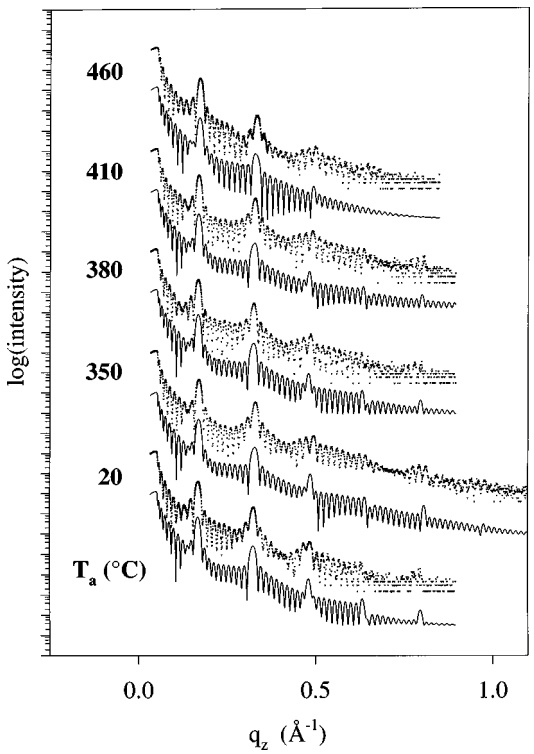

FIG. 2. Specular SA XRD intensity as a function of the vertical scattering vector q_z for all $[\mathrm{Fe}(28\ \text{Å})/\mathrm{Cr}(11\ \text{Å})]_{10}$ superlattices annealed to the temperatures indicated. Shown are the measured data (points) and the simulations (lines). The data show no plateau for the total external reflection at small angles because no footprint correction was applied to the data but instead taken into account in the simulations. All curves are vertically offset for clarity.

(AFF), defined as $\mathrm{AFF}=1-(M_r/M_s)$ with M_r and M_s being, respectively, the remnant and the saturation magnetization, was used to quantify the degree of pin-hole formation introduced by the annealing.

RESULTS AND DISCUSSION

Figure 1 shows the dependence of the magnetoresistance ($\Delta\rho$ and $\Delta\rho/\rho_s$) and the AFF as a function of the annealing temperature T_a. Careful preliminary tests had shown that for $T_a<250$ °C no significant changes in the transport properties occur. At higher temperatures (up to $T_a\approx400$ °C) $\Delta\rho$ and $\Delta\rho/\rho_s$ increase. At even higher temperatures the AFF sharply drops indicating the onset of disintegration of the layered structure. $\Delta\rho$ remains constant whereas $\Delta\rho/\rho_s$ decreases because of the increased contribution of the background resistivity to ρ_s. This behavior is in accordance with studies of the high temperature annealing regime ($T_a>450$ °C) of similar samples showing the suppression of the GMR effect due to the loss of the AF coupling.[24] The low-temperature regime ($T_a\leqslant460$ °C) discussed here is the most interesting part since here the changes in the GMR amplitude must be related to changes in the spin-dependent electron scattering. Moreover, the reason for these changes in the spin-dependent scattering *must* be found in changes of the interface structure since the interfaces are the exclusive source for electron scattering (in the absence of bulk scattering). As mentioned earlier, the interface structure was characterized by specular and diffuse SA XRD using anomalous scattering to enhance the otherwise low contrast in electron density between Fe and Cr. Simulations of the specular and diffuse data reveal, respectively, the vertical component (roughness amplitude η) and the lateral components (lateral correlation length ξ_x and Hurst parameter h of the fractal dimension 3-h) of the interface roughness. The specular data (Fig. 2) show a rich structure including the pronounced superlattice Bragg peaks and the higher frequency Kiessig fringes due to the total film thickness. Already, inspection by eye reveals little variation in the quality of the spectra except for $T_a=460$ °C where the superlattice Bragg peaks are more strongly damped. The simulation of such spectra includes various parameters describing the different interfaces (substrate-film, Fe/Cr, film-oxide, oxide-air) and their separation, i.e., the layer thicknesses. In order to restrict the number of free simulation parameters we used certain input parameters such as the layer thicknesses of Fe and Cr (known from the sample preparation) and the upper oxide layer's composition, typical thickness and roughness (known from independent experiments on single Fe and Cr films[28]). Furthermore, we kept the substrate roughness the same for all simulations. The optical material parameters were taken from Ref. 41. In this way the simulations of the specular SA XRD scans contained the Fe/Cr interface roughness η as the only free parameter. Indeed, the simulations show little variation of η [being constant at (2.95 ± 0.05) Å] for 20 °C $\leqslant T_a\leqslant$ 410 °C and $\eta=4.7$ Å for $T_a=460$ °C. This increased value of η is in agreement with the observed start of the disintegration of the superlattice structure at higher T_a causing also the reduction of the AFF (Fig. 1). Therefore, the vertical component of the interface roughness is obviously not the key for understanding the initial increase of the GMR amplitude (Fig. 1). Thus we have to examine the lateral interface roughness components obtained through analyzing

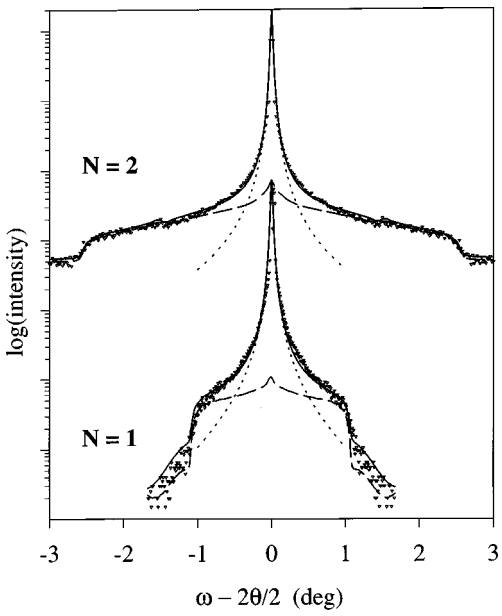

FIG. 3. Diffuse SA XRD intensity as a function of the rocking angle for the unannealed $[\mathrm{Fe}(28\ \text{Å})/\mathrm{Cr}(11\ \text{Å})]_{10}$ superlattice. The spectra were measured with a x-ray wavelength of 2.0753 Å (15 eV below the Cr absorption edge) with q_z at the position of the first ($N=1$) and second ($N=2$) order superlattice Bragg peaks. Shown are the measured data (points), the simulations of the diffuse intensities (dashed lines), the Lorentzian fits to the specular intensities (dotted lines), and the sums of simulated diffuse intensities and fitted specular peaks (full lines). The curves are vertically offset for clarity.

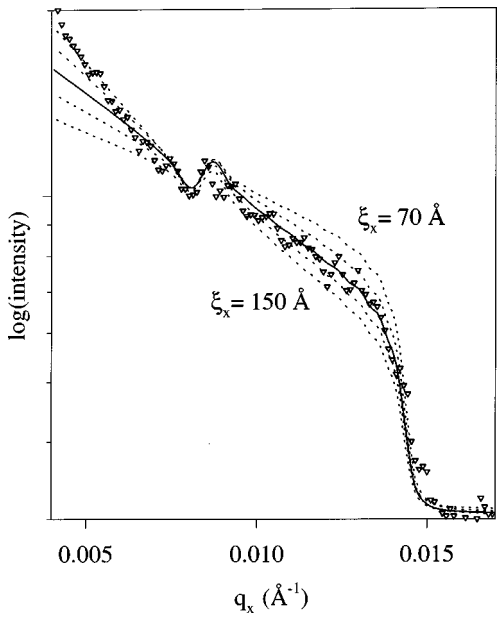

FIG. 4. Diffuse SA XRD intensity as a function of the lateral scattering vector q_x for the not annealed $[\mathrm{Fe}(28\ \text{Å})/\mathrm{Cr}(11\ \text{Å})]_{10}$ superlattice. The spectrum was measured with a x-ray wavelength of 2.0753 Å (15 eV below the Cr absorption edge) with q_z at the position of the second order superlattice Bragg peak. Shown are the measured data (points) and the simulations of the diffuse intensity for various values of ξ_x (70, 90, 110, 130, and 150 Å). The best fit with $\xi_x=110$ Å is shown by a full line.

the ω rocks. A qualitative analysis of such spectra can be misleading since the shape of these curves is determined by several parameters in a rather involved and sometimes counterintuitive way.[33] For the same reasons the quantitative analysis of the spectra has also to be performed with utmost care since a single spectrum can be simulated with different parameter sets. Therefore we will describe in detail the analysis procedure we followed. Reliable data can only be obtained when additional structural information obtained from independent measurements is used. The first crucial point is to separate the specular peak from the diffuse intensity contributions. Ideally, the specular intensity should be sharply peaked around $q_z=0$ (specular condition) but can also be broadened due to some macroscopic substrate surface curvature. The additional (aside from specular) structure parameters determining the diffuse intensity are the lateral correlation length of the substrate-film interface $\xi_x(S)$, the lateral correlation length of the interfaces inside the superlattice ξ_x, the Hurst parameter h and the vertical correlation length ξ_z. From AFM measurements we know that the typical size of the atomically flat substrate terraces is about 1 μm which should yield $\xi_x(S)$ values $\geqslant 1$ μm. Additionally, scanning tunneling microscopy (STM) and AFM studies of single Fe or Cr films[20,42,43] suggest ξ_x values of the order of 100 Å and h values around 0.6. The other parameter ξ_z does not have such a pronounced influence on the q_x dependence of the diffuse intensity. The resulting simulation of the diffuse intensity (dashed lines in Fig. 3) is defined by first, the lateral roughness components of the superlattice interfaces (mostly contributing to the intensity at larger angles, i.e., having a small value of ξ_x of about 100 Å) and second, the lateral roughness component of the substrate surface (responsible for the central small peak in the diffuse intensity, i.e., having a large value of ξ_x of about 1 μm). The remaining difference between measured intensity and simulated diffuse intensity should then be the specular peak which is clearly not sharp around $q_x=0$ (Fig. 3). We can simulate this specular intensity by a Lorentzian intensity distribution (dotted lines in Fig. 3) which reflects imperfections of the polishing procedure of the commercial substrates.[26] This interpretation of the central portion of the ω rock as being the specular intensity is supported by the fact that ω rocks taken at different order superlattice Bragg peaks, are described by Lorentzians with identical width (in ω) as shown in Fig. 3 for 2θ at the first and second order Bragg peak (the diffuse intensity was also simulated with identical parameters). Similar widths of the Lorentzians could be used for all samples. Other combinations of parameters result in values of the roughness parameters which contradict the AFM and STM studies. For the analysis of all ω rocks we kept $\xi_x(S)$ constant at 1 μm (even bigger values would not change the analysis since the central part of the ω rocks is dominated by the specular intensity). The Hurst parameter was found to be around $h=0.5$, however, this value is not defined more precisely by the simulations than within ± 0.2. In order to limit the number of free parameters we kept this parameter constant at $h=0.5$ for all ω rocks. The vertical correlation length ξ_z mostly influences the simulations by rounding the intensity drop off at high q_x values. We found a value of $\xi_z=200$ Å which we also used for all simulations. Therefore, the only free parameter for the simulation of all ω rocks is the lateral correlation length ξ_x. Through careful studies of the influ-

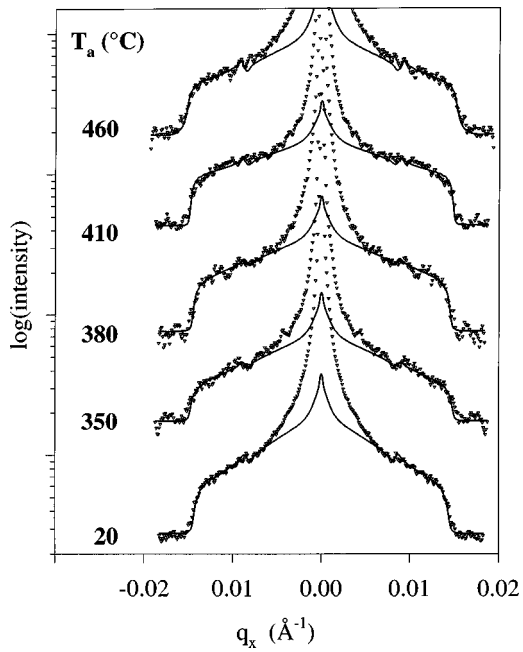

FIG. 5. Diffuse SA XRD intensity as a function of the lateral scattering vector q_x for all $[\mathrm{Fe}(28\ \text{Å})/\mathrm{Cr}(11\ \text{Å})]_{10}$ superlattices annealed to the temperatures as indicated. The spectra were measured with a x-ray wavelength of 2.0753 Å (15 eV below the Cr absorption edge) with q_z at the position of the second order superlattice Bragg peak. Shown are the measured data (points) and the simulations for the diffuse intensities (lines). All curves are vertically offset for clarity.

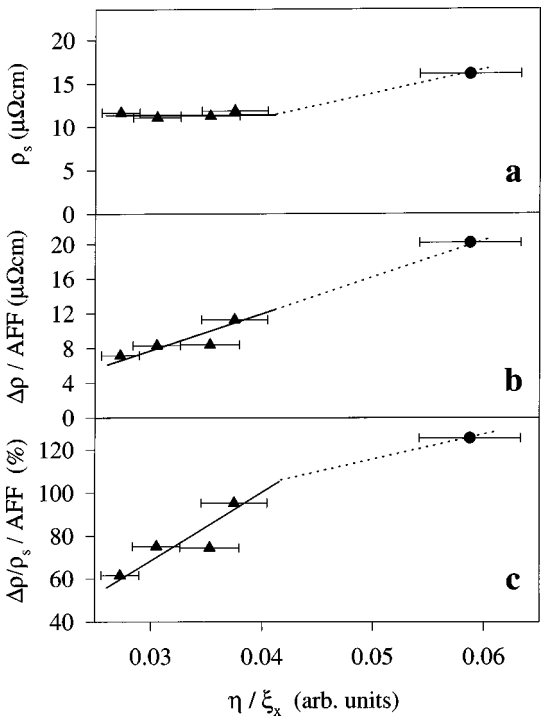

FIG. 7. The transport properties (a) ρ_s, (b) $\Delta\rho$, and (c) $\Delta\rho/\rho$ of the $[\mathrm{Fe}(28\ \text{Å})/\mathrm{Cr}(11\ \text{Å})]_{10}$ superlattices as a function of η/ξ_x which is a structure parameter combining the vertical and lateral interface roughness components. Variations in the AF coupling are taken into account by dividing the magnetoresistance by the AFF. The triangular data points correspond to the samples with constant η and only ξ_x varying. The lines are guides to the eye.

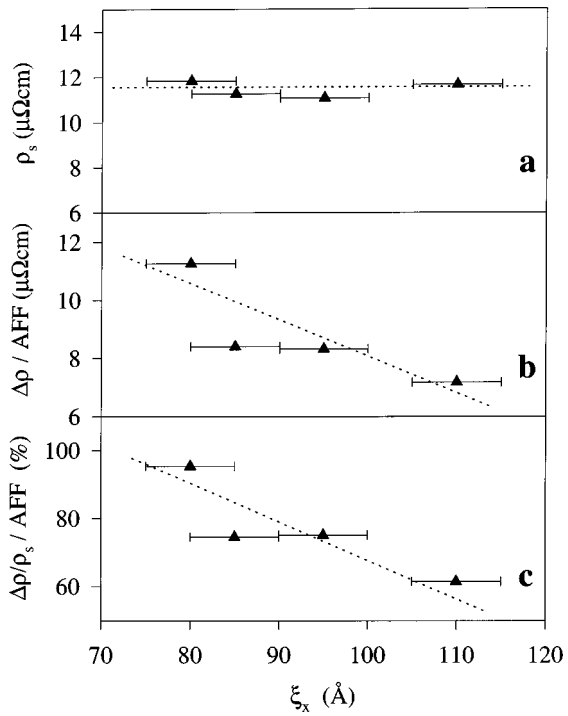

FIG. 6. The transport properties (a) ρ_s, (b) $\Delta\rho$, and (c) $\Delta\rho/\rho$ of the $[\mathrm{Fe}(28\ \text{Å})/\mathrm{Cr}(11\ \text{Å})]_{10}$ superlattices as a function of the lateral correlation length ξ_x. Variations in the AF coupling are taken into account by dividing the magnetoresistance by the AFF. The lines are guides to the eye.

ence of ξ_x on the quality of the simulations (Fig. 4) the error of its value can be estimated. Figure 5 shows the rocking curves taken at the position of the second order superlattice Bragg peak and the simulations describing the diffuse background. It is worth noting also that the spectra's structure around $q_x = \pm 0.008\ \text{Å}^{-1}$ (which is caused by dynamical scattering) is nicely reproduced. The simulations reveal a continuous decrease of ξ_x from 110 to 80 Å with increasing T_a. Obviously the lateral component of the interface structure must dominate the changes in the transport properties.

Next we will link structural information and transport properties of these samples. Theoretical models emphasize the influence of vertical *and* lateral interface roughness parameters. The GMR should increase with both an increasing roughness amplitude or a shrinking lateral correlation length.[6] In our case, we find for moderate annealing temperature up to 400 °C a variation of only the lateral correlation length and an almost constant value of η. The transport data as a function of ξ_x for this annealing temperature regime are shown in Fig. 6. The resistivity ρ_s remains unchanged, however, both absolute ($\Delta\rho$) and relative ($\Delta\rho/\rho_s$) magnetoresistance values decrease with increasing ξ_x. In order to present all data in a single graph, including the ones of the sample with increased η, we combine the vertical and lateral roughness parameters in a single interface roughness parameter η/ξ_x. The saturation resistivity ρ_s [Fig. 7(a)] is constant for small values of η/ξ_x (constant η, triangular data points) and increases for the sample with the increased pin-hole forma-

tion indicating an increase of disorder. At saturation (parallel alignment of the magnetization directions) the charge transport is dominated by the minority electrons. Obviously, these are weakly scattered at the increasing interface step density, as indicated by the decreasing ξ_x. The increase of ρ_s for the highest annealing temperature is more likely caused by the increasing disorder in the form of pin holes. The absolute magnetoresistance $\Delta\rho$/AFF [Fig. 7(b)] increases linearly with increasing η/ξ_x whereas the relative magnetoresistance $\Delta\rho/\rho_s$/AFF [Fig. 7(c)] after an initial steep increase (variations of ξ_x only) grows slower because of the higher value of ρ_s. Clearly, the increasing interface roughness effectively reduces the mobility of the majority electrons leading to the increase of ρ_0 and hence $\Delta\rho$. Since ρ_s is constant, this kind of interface roughness results in a highly spin-selective scattering potential.

CONCLUSIONS

We varied the interface quality of a series of epitaxial Fe/Cr(001) superlattices through annealing at different temperatures. The transport properties of these samples are characterized by negligible bulk scattering thus dominant interface scattering. The interface thickness η and the lateral correlation length ξ_x were quantitatively analyzed by specular and diffuse XRD. For moderate annealing temperatures η is constant whereas ξ_x decreases, indicating a higher step density at the interfaces. We find an increase of the magnetoresistance with decreasing ξ_x at constant ρ_s indicating a high spin selectivity of the electron scattering at annealing-induced interface defects. This study shows clearly the importance of the lateral interface roughness component for the understanding of the spin-dependent transport in magnetic multilayers. At higher annealing temperatures η starts to increase causing a further increase of the GMR amplitude.

This result is in clear contradiction to recently published results measured on *polycrystalline* samples.[19] However, as pointed out in Ref. 19, in spite of the very high GMR amplitudes obtained, the interpretation of the results remained ambiguous because bulk contributions to the spin-dependent scattering could not be separated from the interface contribution. This led to two evenly possible, but opposing, interpretations: one using only the interface contribution and the other being based on a compensation of bulk and interface contributions. Since the results reported here are obtained under elimination of bulk contributions it must be concluded that the transport properties of the *polycrystalline* samples are dominated by bulk scattering. Consequently, no information over the interplay between interface structure and GMR amplitude can be deduced from the properties of such samples.[44]

These structural changes found here for epitaxial Fe/Cr(001) superlattices upon annealing will not necessarily occur in samples of other orientation. First, polycrystalline samples would provide more efficient diffusion channels along grain boundaries facilitating intermixing or pin-hole formation. Furthermore, the thermodynamically stable interface structure will depend on the crystallographic orientation. For instance, (110) oriented Fe/Cr superlattices prefer a zig-zag facetting of the interfaces caused by the formation of (presumably more stable) {100} planes.[45] Accordingly, annealing of (110) textured polycrystalline samples[23,25] might lead to totally different changes in the interface structure.

The dependence of the GMR amplitude on the interface structure, in particular its lateral roughness component, will presumably be the same for all crystallographic orientations. Still, there might be an intrinsic orientation dependence of the size of the GMR effect since different electrons in k space will contribute. However, the experimental verification will be difficult to achieve because of the difficulty in producing samples with different crystallographic orientation but identical interface structure.

ACKNOWLEDGMENTS

This work was financially supported by the Belgian Concerted Action (GOA) and Interuniversity Attraction Poles (IUAP) programs. R.S. and G.V. were supported by the HCM Program of the European Community and the Belgium Interuniversity Institute for Nuclear Sciences, respectively.

*Author to whom correspondence should be addressed. Present address: University of Alabama, Center for Materials for Information Technology, Box 870209, Tuscaloosa, AL 35487. FAX: +1 205 3482346. Electronic address: rschad@bama.49.edu

†Present address: Philips Optical Storage, Kempische Steenweg 293, 3500 Hasselt, Belgium.

[1] M. N. Baibich, J. M. Broto, A. Fert, F. Nguyen Van Dau, F. Petroff, P. Etienne, G. Creuzet, A. Friederich, and J. Chazelas, Phys. Rev. Lett. **61**, 2472 (1988).

[2] M. N. Binasch, P. Grünberg, F. Saurenbach, and W. Zinn, Phys. Rev. B **39**, 4828 (1989).

[3] S. S. P. Parkin, N. More, and K. P. Roche, Phys. Rev. Lett. **64**, 2304 (1990).

[4] R. Q. Hood, L. M. Falicov, and D. R. Penn, Phys. Rev. B **49**, 368 (1994).

[5] Y. Asano, A. Oguria, and S. Maekawa, Phys. Rev. B **48**, 6192 (1993).

[6] J. Barnas and Y. Bruynseraede, Phys. Rev. B **53**, 5449 (1996).

[7] P. Zahn, I. Mertig, M. Richter, and H. Eschrig, Phys. Rev. Lett. **75**, 2996 (1995).

[8] M. Rührig, R. Schäfer, A. Huber, R. Mosler, J. A. Wolf, S. Demokritov, and P. Grünberg, Phys. Status Solidi A **125**, 635 (1991).

[9] C. D. Potter, R. Schad, P. Beliën, G. Verbanck, V. V. Moshchalkov, Y. Bruynseraede, M. Schäfer, R. Schäfer, and P. Grünberg, Phys. Rev. B **49**, 16 055 (1994); R. Schad, C. D. Potter, P. Beliën, G. Verbanck, V. V. Moshchalkov, Y. Bruynseraede, M. Schäfer, R. Schäfer, and P. Grünberg, J. Appl. Phys. **76**, 6604 (1994).

[10] J. C. Slonczewski, Phys. Rev. Lett. **67**, 3172 (1991).

[11] J. C. Slonszewski, J. Appl. Phys. **73**, 5975 (1993).

[12] Kees M. Schep, Paul J. Kelly, and Gerrit E. W. Bauer, Phys. Rev. Lett. **74**, 586 (1995).

[13] C. T. Yu, K. Westerholt, K. Theis-Bröhl, and H. Zabel, J. Appl. Phys. **82**, 5560 (1997).

[14] E. E. Fullerton, D. M. Kelly, J. Guimpel, I. K. Schuller, and Y. Bruynseraede, Phys. Rev. Lett. **68**, 859 (1992).

[15] N. M. Rensing, A. P. Payne, and B. M. Clemens, J. Magn. Magn. Mater. **121**, 436 (1993).

[16] N. M. Rensing, B. M. Clemens, and D. L. Williamson, J. Appl. Phys. **79**, 7757 (1996).
[17] P. Beliën, R. Schad, C. D. Potter, G. Verbanck, V. V. Moshchalkov, and Y. Bruynseraede, Phys. Rev. B **50**, 9957 (1994).
[18] S. Joo, Y. Obi, K. Takanashi, and H. Fujimori, J. Magn. Magn. Mater. **104**, 1753 (1992).
[19] R. Schad, P. Beliën, G. Verbanck, C. D. Potter, H. Fischer, S. Lefebvre, M. Bessiere, V. V. Moshchalkov, and Y. Bruynseraede, Phys. Rev. B **57**, 13 692 (1998).
[20] R. Schad, P. Beliën, G. Verbanck, C. D. Potter, K. Temst, V. V. Moshchalkov, and Y. Bruynseraede, J. Magn. Magn. Mater. **182**, 65 (1998).
[21] R. Schad, P. Beliën, J. Barnas, G. Verbanck, C. D. Potter, G. Gladyszewski, V. V. Moshchalkov, and Y. Bruynseraede, J. Magn. Magn. Mater. **156**, 341 (1996).
[22] F. Petroff, A. Barthelemy, A. Hamzic, A. Fert, P. Etienne, S. Lequien, and G. Creuzet, J. Magn. Magn. Mater. **93**, 95 (1991).
[23] N. M. Rensing and B. M. Clemens, in *Magnetic Ultrathin Films: Multilayers and Surfaces/Interfaces and Characterization*, edited by B. T. Jonker *et al.*, MRS Symposia Proceedings No. 313 (Materials Research Society, Pittsburgh, 1993), p. 197.
[24] H. Laidler, B. J. Hickey, T. P. A. Hase, B. K. Tanner, R. Schad, and Y. Bruynseraede, J. Magn. Magn. Mater. **156**, 332 (1996).
[25] J. M. Colino, I. K. Schuller, V. Korenivski, and K. V. Rao, Phys. Rev. B **54**, 13 030 (1996).
[26] MgO substrates purchased from Kristallhandel Kelpin, Leimen (Germany).
[27] W. Sevenhans, J.-P. Locquet, and Y. Bruynseraede, Rev. Sci. Instrum. **57**, 937 (1986).
[28] R. Schad, D. Bahr, J. Falta, P. Beliën, and Y. Bruynseraede, J. Phys.: Condens. Matter **10**, 61 (1998).
[29] R. Schad, C. D. Potter, P. Beliën, G. Verbanck, V. V. Moshchalkov, and Y. Bruynseraede, Appl. Phys. Lett. **64**, 3500 (1994).
[30] B. Vidal and P. Vincent, Appl. Opt. **23**, 1794 (1984).
[31] J. Daillant and O. Belorgey, J. Chem. Phys. **97**, 5824 (1992).
[32] Henry E. Fischer, memoire DHDR (Diplome d'Habilitation a Diriger les Recherches), Université Joseph Fourier (Grenoble, France).
[33] H. E. Fischer, H. M. Fischer, and M. Piecuch (unpublished).
[34] H. E. Fischer, H. Fischer, O. Durand, O. Pellegrino, S. Andrieu, M. Picuch, S. Lefebvre, and M. Bessiere, Nucl. Instrum. Methods Phys. Res. B **97**, 402 (1995).
[35] L. Nevot and P. Croce, Rev. Phys. Appl. **15**, 761 (1980).
[36] E. E. Fullerton, I. K. Schuller, H. Vanderstraeten, and Y. Bruynseraede, Phys. Rev. B **45**, 9292 (1992).
[37] S. K. Sinha, E. B. Sirota, S. Garoff, and H. B. Stanley, Phys. Rev. B **38**, 2297 (1988).
[38] V. Holý, J. Kubeña, I. Ohídal, K. Lischka, and W. Poltz, Phys. Rev. B **47**, 15 896 (1993).
[39] V. Holý and T. Baumbach, Phys. Rev. B **49**, 10 668 (1994).
[40] J.-P. Schlomka, M. Tolan, L. Schwalowsky, O. H. Seeck, J. Stettner, and W. Press, Phys. Rev. B **51**, 2311 (1995).
[41] S. Brennan and P. L. Cowan, Rev. Sci. Instrum. **63**, 850 (1992).
[42] J. F. Lawler, R Schad, S. Jordan, and H. van Kempen, J. Magn. Magn. Mater. **165**, 224 (1997).
[43] S. Jordan, R. Schad, J. F. Lawler, D. J. L. Herrmann, and H. van Kempen, J. Phys.: Condens. Matter **10**, L355 (1998).
[44] Since other studies neglected the (supposedly non-negligible) bulk scattering, and were based on samples with only about 10% GMR amplitude without providing a quantitative and complete structure analysis, a comparison with those results is not possible.
[45] W. Folkerts and F. Hakkens, J. Appl. Phys. **73**, 3922 (1993).